Refining the Search for Sub-threshold Lensed Gravitational Waves
LIGO SURF 2021 Interim Report 2

Storm Colloms,[1, a]
Mentors: Alvin Li,[2, b] and Alan J. Weinstein[2, c]
[1]*School of Physics and Astronomy, University of Edinburgh*
[2]*LIGO Laboratory, California Institute of Technology*
(Dated: July 29, 2021)

Gravitational waves, theorised over 100 years ago, open up a new window with which to study the universe. Since their first detection with LIGO (Laser Interferometer Gravitational-wave Observatory) in 2015, properties of gravitational waves such as their speed, polarisation, and weak interaction with matter have been observed, and many properties of their sources investigated. Like the gravitational lensing of light due to curved space-time caused by massive bodies, gravitational waves can also be lensed. Gravitational lensing would produce multiple events of the gravitational waves which are magnified or de-magnitfied and time-delayed compared to what would be the unlensed wave. De-magnified lensed counterparts may be present in data from recent LIGO observing runs but could be undetectable with current signal analysis methods due to the high noise background. I propose a project to make improvements to targeted sub-threshold lensed gravitational wave search pipeline, which would include investigating the waveform approximant used in the pipeline, as well as imposing conditions on the sky location of the lensed images.

1. INTRODUCTION

In 2015 almost 100 years since they were first predicted, gravitational waves resulting from a pair of merging black holes were detected with the Advanced Laser Interferometer Gravitational-Wave Observatory (aLIGO) for the first time [1]. Since the first detection of propagations of energy through spacetime, there have been on the order of of 50 detection events over two and a half observing runs, with the number of detections increasing between each observing run as the instrument sensitivity and data analysis techniques are improved [2, 3].

Gravitational lensing has first been observed in the case of electromagnetic light, as seen by Sir Arthur Eddington in 1919 with the measured lensing of light from stars around the eclipsed sun [4]. General relativity's equivalence principle says this lensing should also occur for gravitational waves yet this has not been observed despite many efforts. Gravitational lensing is the one of the fundamental properties of gravitational waves predicted by general relativity not yet to have been observed, others that have been observed include their speed, polarisation, and weak interaction with matter, as well as higher order modes.

Efforts have been made to identify lensed gravitational waves within the current LIGO catalogues [5–11]. With the expected rate for lensing and the increasing gravitational wave detections, it is very likely that recent or near future data from LIGO will contain strongly lensed gravitational waves. This would allow not only insight into comparisons of observations of lensing with general relativity, but allow investigations into the structure of the universe and its matter distribution, such as probing the population of intermediate mass black holes [12].

Strong lensing creates multiple images of the lensed wave, and provided that the wavelength of the gravitational wave is much smaller than Schwarzschild radius of the lens, the magnification due to gravitational lensing will not depend on the gravitational wave's frequency [13]. This means the wave profile of the lensed counterparts and the wave if it were not lensed would be the same apart from an overall scaling factor. Some of these lensed signals may be considered sub-threshold waves which would be buried in the noise background and thus have not previously been detected.

This report is structured as follows: the background section details the properties of gravitational wave, the methods of detection and signal processing, lensing of electromagnetic light as gravitational waves, and what efforts have been made so far to detect lensing from gravitational wave data. Section 3 then details the aims of the project, and section 4 poses a time plan of when to carry out the said objectives. Section 5 details the first portion of work on the project, detail method results and conclusions.

2. BACKGROUND

Gravitational Waves

Gravitational waves were theorised to be self-propagating ripples in spacetime caused by accelerating masses, predicted by Einstein's theory of general relativity in 1916 [14]. The weak-field gravitational equation (equation 1) gives solutions of the form in equation 2 in the absence of mass, the form of these evidently hints at gravitational waves which stretch and squeeze the fabric of spacetime as they travel:

$$\Box h_{ij} = -\frac{16\pi G}{c^4} T_{ij} \,, \tag{1}$$

$$h_{ij}(t) \propto exp(i\vec{k}\cdot\vec{x} - kct) \tag{2}$$

where G is the gravitational constant, c is the speed of light in a vacuum, T_{ij} is the stress-energy tensor, $\vec{k}$ is the wave vector, $\vec{x}$ the direction in which it is travelling, and t time. These solutions predict the speed of these waves as c, which has been verified with observed gravitational waves to be true to within -3×10^{-15} and $+7\times10^{-16}$ times the speed of light [15]. The form of the spacetime strain can also be expressed in terms of its Fourier transform from the frequency domain $\tilde{h}_A$, as observed at a detector:

$$h_{ij}(t,\vec{r}) = \sum_{A=+,\times} e^A_{ij}(\hat{n}) \int_{-\infty}^{+\infty} \tilde{h}_A(f) e^{-i2\pi f(t-\frac{\hat{n}\cdot\vec{r}}{c})} \tag{3}$$

where the gravitational wave strain is split across two polarisations, h-plus (h_+) and h-cross ($h_\times$). As a gravitational wave passes through a ring of test masses, the ring can be seen to be deformed as in figure 1. Under gauge freedom, choosing the transverse-traceless gauge confines the deformations to the x-y plane where the wave propagates in the z direction. Therefore the tensors $e_{ij}(\hat{n})$ are the polarisation tensors for the wave. The transverse traceless gauge also means the retarded time $t - \frac{\hat{n}\cdot\vec{r}}{c}$ can be simplified to simply t as the gravitational wave wavelength is much longer than the detector arm length $\vec{r}$. The resultant spacetime strain h_{ij} is a linear combination of these polarisations, giving the form of the deformations to be linear, circular, or elliptical.

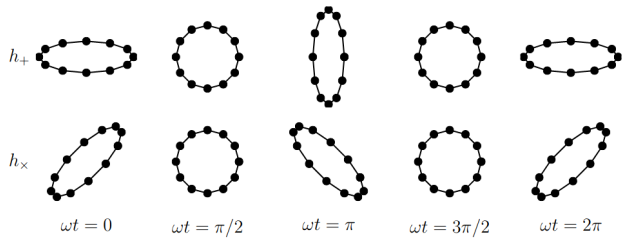

Figure 1. A ring of free-falling test masses as deformed by h_+ (above) and $h_\times$ (below) polarisations of a gravitational wave throughout one period of oscillations. It can be seen that the deformation from the $h_\times$ polarisation is at a 45 degree angle to the h_+ polarisation. Figure From [16].

Detection of Gravitational Waves

Gravitational waves were first detected by aLIGO (Advanced Laser Interferometer Gravitational-Wave Observatory) on the 14th of September 2015 [17]. LIGO uses a Michelson-Morley interferometer, which measures the strain of the waves due to differences in the perpendicular arm lengths of the detector. A laser beam is split into the two arms by a beam splitter, the laser light then travels down the arms of length 4km and is reflected off mirrors at the end of each arm. To increase the path length to that which is needed for the required frequencies the light is reflected multiple times up and down the arms with Fabry-Perot cavities. Light recombines at a detector to usually produce destructive interference in the absence of noise or gravitational wave strain. In the presence of a gravitational wave the arms of the detector will oscillate in length, the difference in arm length given by the strain h_{ij} times the arm length. Under the transverse-tracless gauge, the mirrors can be treated as free-falling, meaning the length of the arms does not change under a the wave strain and instead the time taken for the light to travel down the arm oscillates, thus the phase difference between the light at recombination will also oscillate. This changing phase difference is then used to measure the strain of the signal.

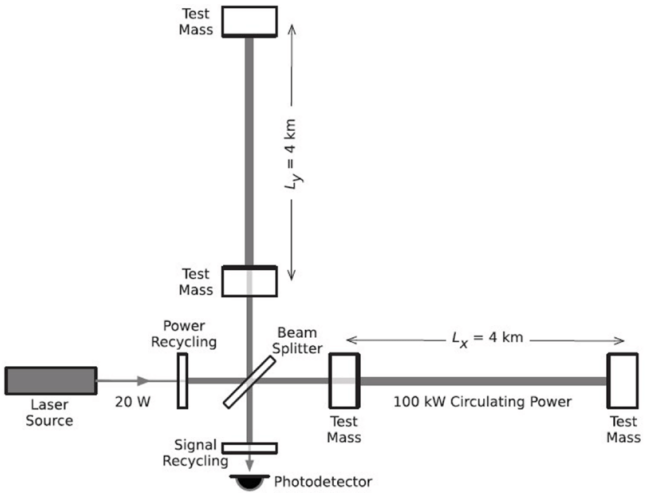

Figure 2. A simplified diagram of the Michelson Morley interferometer located at the LIGO sites. Laser to beam splitter, 4km arms light reflected multiple times in Fabry-Perot cavaties. The light recombines at the detector, which is set to deconstructive interference under the absence of noise of a gravitational wave signal. Figure from [18].

There are two LIGO detectors in Hanford and Livingston in the USA, and a third detector, VIRGO in Italy. The multiple detectors can be used to confirm signals across the three locations, providing the time difference between the events is at most the distance separating them divided by the speed of the waves. If the same signal is being observed in more than one detector within a certain time window, the likelihood of the event can be improved. Such criterion is known as the coincidence criterion. This can strengthen the confidence that the event is a true signal, as well as localise the signal's origin and disentangle its polarisations.

Ground based detectors are tuned to detect gravitational wave frequencies in range from $\sim$20 hertz to several kilohertz. Abundance of noise in the detectors makes it challenging to detect signals outwith this range, where there is a dip in the

median noise frequency distribution, as seen in figure 3. The current sensitivity of the detectors allows gravitational noise strain to be detected down to strains of order $10^{-23}\ 1/\sqrt{Hz}$ around frequencies of 100 Hz.

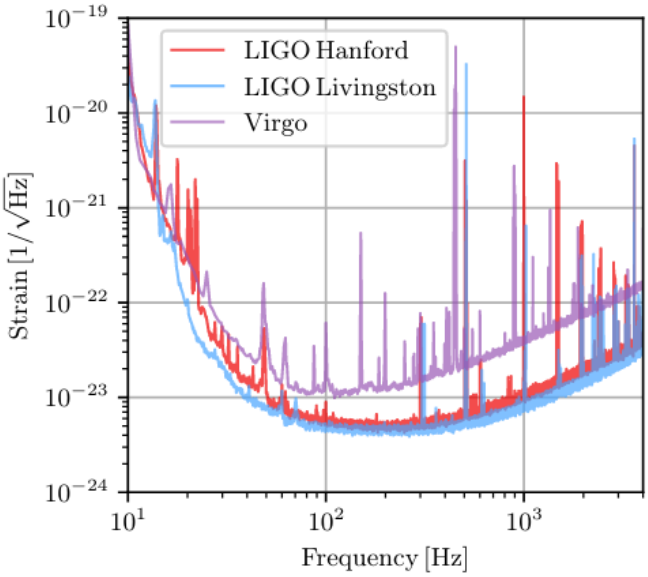

Figure 3. The spectral frequency distributions of strain noise in LIGO and Virgo as of 2019. The lower frequencies are increasingly dominated by seismic and ground noise, while quantum noise dominates at higher frequencies. A so-called bucket can be seen around 100Hz, where current observations occur. Figure from [3]

The operating frequency of these detectors corresponds to the typical frequency ranges of the inspiral, merger, and ringdown phases of compact binary coalescences (CBCs) in the stellar mass range, which can be categorised into merging events of binary black holes (BBH), binary neutron stars (BNS), or one of each (NSBH). The gravitational waves in the inspiral phase carry away energy, reducing the separation of the objects and their angular momentum. The merger phase occurs at the peak amplitude of the event in the time domain as seen in figure 4, when the sources coalesce into one body. Finally the body will release further gravitational waves while stabilising from the merging event. These three stages, inspiral, merger, and ringdown, together constitute a coalescence and are shown in figure 4.

The first event at aLIGO on the 14th of September 2015 was the merging event of two stellar mass black holes (GW150914) [18], and since then approximately 50 further mergers have been identified from neutron stars around several solar masses large up to black holes as massive as several hundreds of solar-masses [2][3].

Other predicted sources of gravitational waves include stochastic background from wide range of sources far away;

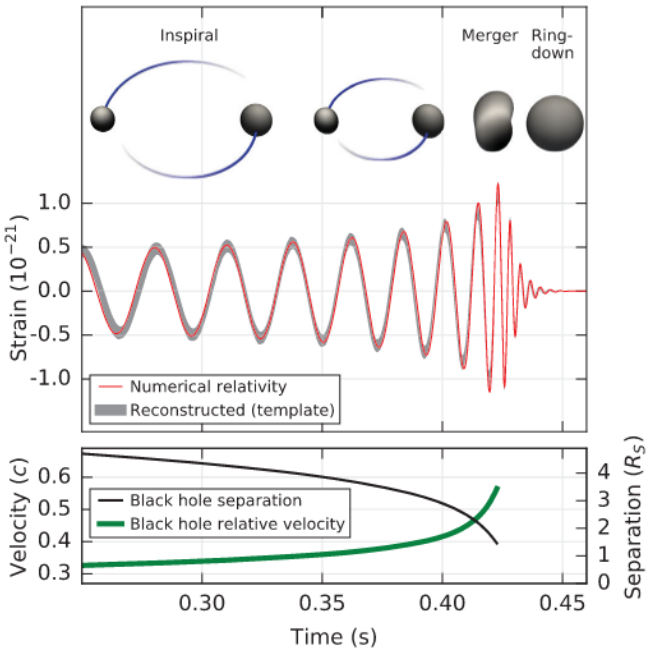

Figure 4. The strain of gravitational wave GW150914 versus time alongside a graphic depiction of the inspiral, merger, and ringdown phases (top). The bottom panel shows the black hole relative velocity, which increases exponentially until the merger phase, and the black hole separation which decreases until the same point. Figure from [18].

continuous waves which could be propagating from rotating neutron stars that are not perfectly spherical; and burst gravitational waves which encapsulates waves from poorly modelled source [19].

While these mergers are some of spacetime's most violent events, the gravitational waves spread across spacetime until they are detected on Earth. The amplitude of the strain of these gravitational waves is thus reduced from the time of the event, and then measured as the fractional change in arm length in the detectors, i.e. the ratio of spacetime distortion. For the current observations, this strain is of order $h(t) = D^{ij}h_{ij}(t) \sim 10^{-21}$ or smaller, where D^{ij} is a constant tensor that depends on the geometry of the detector.

To be able to detect the strains of gravitational waves above noise in the detector, efforts have been made to improve the detector sensitivity and reduce the noise. Noise sources include quantum, seismic, and thermal noise over large frequency bands, as well as fixed frequencies of noise such as 60Hz mains power lines which constitute the spectral lines in figure 3. Noise such as seismic noise from earthquakes can be identified and removed by comparing real time data from seismometers and microphones to the strain data received at the laser detector. Despite efforts to remove many of the noise sources, strain data from gravitational waves still remains

"hidden" behind the noisy data, as seen figure 5. The main aim of gravitational wave signal analysis is then to be able to distinguish the gravitational wave from the background noise.

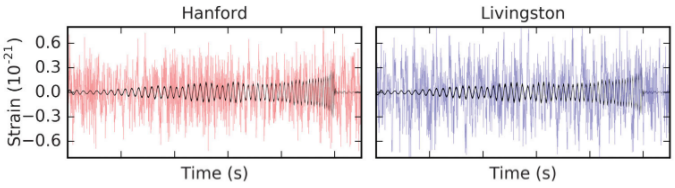

Figure 5. The strain data versus time for gravitational wave GW151226 in the Hanford and Livingston detectors, filtered with a 30–600 Hz bandpass filter to remove large fluctuations in strain outside this frequency range, shown in blue and red. Shown in black is the waveform of the gravitational wave of the strain data for the wave with best fitting parameters to the data. It can be seen that the noise is much greater than the wave strain, thus matched filtering is needed to extract the waveform. Figure from [20].

Signal Processing

Despite efforts to reduce noise, the noise is still much larger in magnitude than the typical gravitational wave. Therefore, the approximate shape of the waveform must be found to be able to compare with the data. This is called matched filtering. The shape of the waveform can be determined by 15 parameters of the coalescence; 8 intrinsic parameters: the mass of each coalescing body m_1 and m_2, their spins $\vec{S_1}$ and $\vec{S_2}$; and 7 extrinsic parameters: the time of coalescence t_c, the reference phase φ_c, the sky position in right ascension and declination α and δ, luminosity distance d_L, and the orbital orientation Θ_{Jn}, ψ. Additionally neutron stars can be characterised by another parameter, tidal deformability $\tilde{\Lambda}$ for the total of 16 parameters.

In order to find a gravitational wave event, the signal-to-noise ratio (SNR), a measure of the strength of the signal assuming it matches a given template, can be maximised for a range of templates, hence finding the best fitting template. While the parameters that determine the waveforms of the templates are continuous, the templates used to perform matched filtering are discrete and the collection of templates is named the template bank.

The data received at the detector $s(t)$ is given by the addition of the noise signal $n(t)$ and the gravitational wave signal $h(t)$:

$$s(t) = n(t) + h(t)\ . \tag{4}$$

For a given filter with filter function $P(t)$, which gives the whitened function of the template, the matched filtering output can be given by:

$$\hat{s} = \int s(t)P(t)dt\ . \tag{5}$$

The SNR can then be defined as the expectation value of the matched filtering output when a signal is present, $\langle S\rangle$ divided by the root mean square of the output when there is no GW signal, N:

$$\rho = \frac{\langle S\rangle}{N}\ , \tag{6}$$

where $\langle S\rangle$ can be found with:

$$\langle S\rangle = \int \langle s(t)P(t)\rangle dt \tag{7}$$

$$= \int \langle (n(t)+h(t))P(t)\rangle dt \tag{8}$$

$$= \int \langle h(t)P(t)\rangle dt \tag{9}$$

$$= \int \tilde{h}(f)\tilde{P}^*(f)df. \tag{10}$$

Here $\langle n(t)\rangle$ can be taken as zero assuming the noise is both Gaussian and stationary. This is can be assumed to be the case under the assumption that no glitches, disruptions in the Gaussian and stationary nature of the noise, occur.

N is then:

$$N^2 = \langle \hat{s}^2\rangle - \langle \hat{s}\rangle^2 \tag{11}$$

$$= \langle \hat{s}^2\rangle \tag{12}$$

$$= \int\int P(t)P(t')\langle n(t)n(t')\rangle dtdt' \tag{13}$$

$$= \frac{1}{2}\int S_n(f)|\tilde{P}^*(f)|^2 df \tag{14}$$

where S_n is the power spectral density of the noise, or the power distribution in the noise among all frequency components.

If a signal then matches with a template to create a high SNR at a certain time in the data, it is then called a trigger. SNR based ranking of signals is a good starting point, however it cannot be used solely as it assumes that the noise is Gaussian and stationary. In the case of noise glitching and non-stationarity, a false-alarm rate (FAR), which signifies the rate that noise could produce the trigger under consideration, amongst other ranking statistics can be introduced [21, 22].

GstLAL

GstLAL is one of the pipelines for matched filtering and data reduction of the gravitational wave data. The pipeline can be performed either offline once all of the data has been recorded, or low-latency i.e. with minimal delay from the recording of the data. Low-latency methods allow for rapid electromagnitic follow-up of any candidate gravitational waves. The primary steps in the offline mode of the GstLAL pipeline are shown in figure 6.

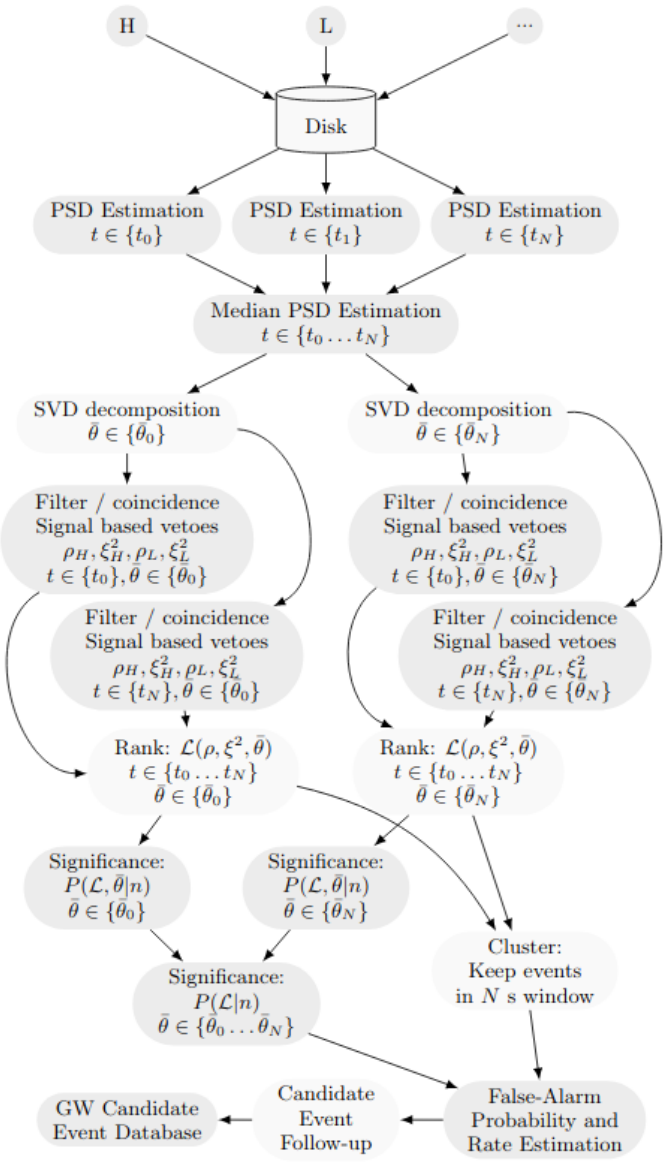

Figure 6. Diagram of the offline search mode of the GstLAL pipeline, following data retrieval, PSD estimation, filtering and ranking, and follow-up parameter estimation. Figure from [22]

After the data has been received and recorded from the 3 detectors, the first step in the pipeline is to estimate the PSD for the chunk of data. Above, the PSD was found directly from the equation:

$$\langle \tilde{n}(f)\tilde{n}*(f')\rangle = \frac{1}{2}S_n(f)\delta(f-f'). \quad (15)$$

However this cannot be used for real data as it may contain an actual signal and not just noise, and will also contain glitches which would make the noise non-Gaussian non-stationary. Therefore the data is split into small time slices and Fourier transformed into the frequency domain, from which the median of these is taken to to be the median PSD for said chunk of data [22].

The data series is then whitened by dividing by the square root of the PSD. The amplitude of the data is scaled so that variance of the data amplitude is then 1. If there is any point in the whitened data that has a variance exceeding a certain value it can be said to be a glitch and can be removed by zeroing the data around that point to 0.25s either side, in a process known as gating. This removes obvious glitches that would create high SNR triggers in the data. Alternatively, if there is a known source of glitched data from instrumental and environmental monitors at the detectors, such as an earthquake, this can be flagged so the data can be vetoed (set to zero) around this time.

Since the template bank is discrete yet the parameters of gravitational wave signals are continuous, if a signal occurs that does not exactly match a filter this can incur a loss of SNR. In matched filtering, this can be mitigated by reducing the number of templates, which is done by reducing templates to vectors which match part of the signal. This is known done as the LLOID process, which encompasses chopping templates into different time slices, down sampling each slice, and single-value decomposition (SVD). The total SNR for each trigger is then found from the total of the SNR from the top select eigenvectors.

In addition to SNR, each trigger must be categorised by the difference between the trigger and the matched filter, ξ^2. This allows for further distinction between glitches and true signals, as a high SNR trigger may not truly match well to the filter in other coalescence phases outwith the high-amplitude and thus high SNR merger phase.

The SNR (ρ) and the ξ^2 of the triggers, as well as the filter parameters $\bar{\theta}$ can be used to determine the log-likelihood ratio $\mathscr{L}$, given by equation 17:

$$\mathscr{L}(\rho_1, \xi_1^2, ..., \rho_d, \xi_d^2, \bar{\theta}) = \frac{P(\rho_1, \xi_1^2, ..., \rho_d, \xi_d^2, \bar{\theta}|s)}{P(\rho_1, \xi_1^2, ..., \rho_d, \xi_d^2, \bar{\theta}|n)}, \quad (16)$$

for number of detectors d, and where $P(...|s)$ is the probability of observing the trigger (...) given a signal, and $P(...|n)$ is the probability of observing (...) given noise.

The false alarm probability, $P(\mathscr{L}|n)$, can also be calculated as the probability of measuring a given $\mathscr{L}$ if the data contains only noise. From this, the probability of obtaining a trigger of log-likelihood ratio greater than a certain threshold $\mathscr{L}*$ may be found by integrating the false alarm probability from this threshold to infinity. The false alarm rate (FAR), defined as how often the noise is expected to yield an event with a log likelihood greater than this threshold, can be calculated by dividing this cumulative probability by the observing time:

$$FAR = \frac{\int_{\mathscr{L}*}^{\infty} d\mathscr{L} P(\mathscr{L}|n)}{T}, \quad (17)$$

where T is the observing time.

If the trigger is detected in more than one detector then its ranking is promoted, however single detector triggers can still by ranked highly while incurring a penalty.

Following the final ranked list of triggers, the highest ranking triggers undergo follow-up parameter estimation using Bayesian analysis. Since the parameters estimated from matched filtering are just those best fitting to the template, parameter estimation gives more reliable results for 15 (16 for a neutron star) parameters of the CBC.

Lensing

Another consequence of the bending of spacetime is that of gravitational lensing. As light travels on the shortest path through spacetime, it's path may be curved by curved spacetime. This can cause the apparent position of the bent light source to change according to an observer on the other side of the lens, as seen in figure 7.

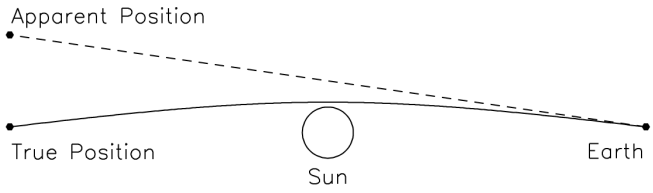

Figure 7. The bending of radiation around a massive object, here the sun, to reach an observer on Earth who would presume the light has travelled in a straight line, hence altering the source objects apparent position from its true position. Figure from [23].

Strong lensing also effects the arrival time of the light due to the speed of light changing through curved spacetime, as well as due to the difference in path lengths for different images. Multiple images are also created under this lensing regime, as the slight differences in the directions of the light from the source will be bent by different angles. These images will have different arrival times due to the difference in path lengths between the differently lensed components. Gravitational lensing of electromagnetic light has been observed extensively, as seen with Eddington's eclipse experiment in 1919 as well as phenomena such as Einstein rings captured by the Hubble Space Telescope.

Under the equivalence principle, gravitational lensing should also occur for gravitational waves. While lensing of light may be obscured due to dust between the lensed source and the observer, this is not a problem for gravitational waves which are not impacted by the obscuring matter. This means that the observations of lensed gravitational waves could allow further probing of the structure of the universe that cannot be gathered from the lensing of light.

The strain of the lensed gravitational wave can be related to the strain of the unlensed gravitational wave:

$$h_{+,\times}^{lensed}(f) = F(f) h_{+,\times}^{unlensed} \quad (18)$$

where $F(f)$ is the amplification function that depends on the frequency of the wave, as well as parameters such as the lens mass and the distances between the observer, the lens and the source [13]. Two forms of this function can be found by with two simple models, taking the lens as a point-mass, or a singular isothermal ellipsoid (SIE), although these are vastly simplified and not comparable to real astrophysical lenses. These models create two or four images of the lensed wave, with different amplifications and time delays.

Assuming the geometric optics limit holds such that the wavelength of the gravitational waves is much smaller than the Schwarzschild radius of the lens, $F(f)$ can be shown to be independent of the frequency of the wave, instead solely modifying the wave's amplitude and phase [13]. This is also known as the lensing being achromatic. This limit holds in the cases with stellar mass coalescing source objects being lensed by massive objects such as supermassive black holes or star clusters, but breaks down in the case of merging events from supermassive black holes lensed by similarly massive objects, or when stellar mass sources are lensed by intermediate black holes of mass $\sim 10^3 M_{\odot}$. However, for the LIGO frequency band, it is expected that any lensed events observed would be able to approximated by the geometric optics limit.

Received at the detector, this amplitude modification scales the SNR of the lensed wave, as seen in figure 8. The SNR is also inversely proportional to luminosity distance, thus new matched filtering templates of lensed waves can be created by scaling existing templates to be at larger distances, i.e. pushing them further away, reducing their SNR and mirroring the effect of the above $F(f)$ function.

For the case of two lensed images, The probability distribution of the amplification factor has been found to differ between each image, one being very likely to be demagnified while the other magnified to typically a factor of 4 [8]. The typical time delay between these images would also be on the order of minutes, although could be as long as weeks, or months [8, 24, 25].

The expected rate of lensing of gravitational waves is $0.2^{+1.0}_{-0.1}\,\mathrm{yr}^{-1}$ at LIGO's current sensitivity, which would rise to $5^{+5}_{-3}\,\mathrm{yr}^{-1}$ at LIGO's design sensitivity limit [26]. Another study predicts that 30% of lensed waves would be of the 4 image type [25]. These statistics make it highly likely that LIGO

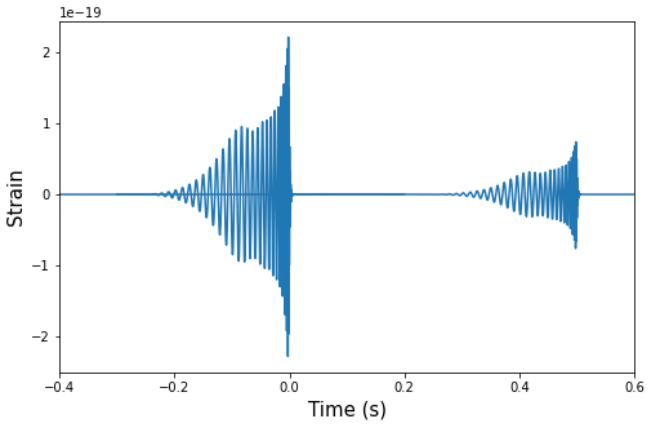

Figure 8. Waveforms of lensed counterparts plotted with waveform template family IMRPhenomPv2. The gravitational wave source is a CBC of two masses of 10 $M_\odot$ and 20 $M_\odot$, spins of 0.9 and 0, at luminosity distance 1 Mpc. The inspiral stage of these counterparts would actually last much longer than 0.2s, but the start of the waveform is tapered in at this time to avoid overlapping waveforms of multiple events, extra computational work in producing such long data, and having an abrupt start which would produce Gibbs noise in any Fourier transforms. The dimensionless source position relative to the central axis passing through the observer and the lens is 0.5, giving the ratio of magnifications to be ~ 3 assuming a point mass lens; and the time delay for a lens of mass $2.5 \times 10^4\ M_\odot$ is as shown 0.5 seconds [13]. The magnified counterpart arrives before the de-magnified wave, which is shorter than the expected delay for lensed images of gravitational waves. It can be seen that the overall amplitude of the lensed waves are modified by the lensing but their frequency profile is identical. If these waves were captured in noise and the SNR versus time were plotted, the first magnified wave might have high enough SNR to surpass the trigger threshold, with the de-magnified counterpart could be buried, making it sub-threshold.

data will contain or has already contained evidence of lensed waves, giving strong motivation to pursue this search.

Searches So Far

The first 11 events in observing runs O1 and O2 have been investigated for three pieces of evidence of lensing: gravitational wave magnifications altering the redshift and chirp mass distribution of the detected BBHs; super-threshold pairs of gravitational waves; and instances of wave optics effects in the waveform of the signals where the geometric optics limit did not hold [5]. No evidence for lensed gravitational waves was identified with these methods.

Furthermore, multiple techniques have been used to search for "sub-threshold" waves which have been lensed to a weaker amplitude, or de-magnified [6, 7]. The results from [6] show no evidence of lensed waves, while those from [7] still require parameter estimation to claim the candidates as lensed waves.

The sub-threshold waves are considerably smaller than the noise-background and thus require further digging to extract them. This includes reducing the noise background by decreasing the templates in the template bank, without reducing the ability to detect the gravitational wave signal.

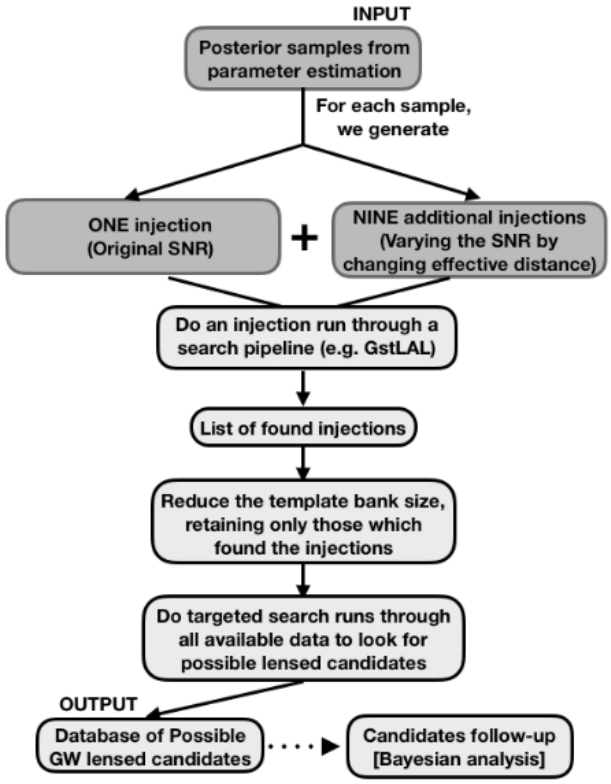

Figure 9. The pipeline to search for sub-threshold gravitational waves as used in [7]. The template bank is reduced by injecting signals with altered and original SNR into the data and only preserving the templates which recover these injections. The new template bank is used to search through all the data, which now has a reduced noise background due to the reduced template bank. Follow-up then needs to be performed on the candidates from this targeted search. Figure from [7].

3. OBJECTIVES

In this project I will continue the search for sub-threshold lensed gravitational waves. The current targeted sub-threshold search (TESLA) pipeline, as shown in figure 9, could be improved in several areas in order to improve its efficiency and improve the chances of finding evidence of a lensed gravitational wave.

The waveform template family used in this pipeline for creating the matched filtering templates in identifying sub-threshold gravitational waves is the spin-aligned approximant IMR-PhenomD. However, using a different waveform

approximant may alter the reduced template bank and any possible candidates. I aim to understand the difference between several approximants, and investigate the outcome of these on the targeted sub-threshold search for strongly lensed gravitational waves pipeline in order to find what the optimal waveform approximant is.

Furthermore, lensed gravitational waves will come from approximately the same sky location. Thus another constraint can be placed on the search pipeline to give lower ranking statistics to waves with lensed counterparts of wide separation. This can be integrated into the pipeline due to the more recent log likelihood ratio dependencies on the differences in coalescence phase $\Delta\phi$ and time Δt between detectors [21]. For each set of two detectors, this can be defined as:

$$\mathscr{L} = \frac{P(\{D_1,D_2\}\{d_1,d_2\},\rho_1,\rho_2,\xi_1^2,\xi_2^2,\Delta\phi,\Delta t|signal)}{P(\{D_1,D_2\}\{d_1,d_2\},\rho_1,\rho_2,\xi_1^2,\xi_2^2,\Delta\phi,\Delta t|noise)}, \tag{19}$$

where D_i is the horizon distance to the d_ith detector, ρ_i is the SNR and ξ_i^2 in said detector.

Δt and $\Delta\phi$ depend on the sky location of the source and the positions of the detectors, as a wave coming from a different direction relative to the line between the pairs of detectors will have different times of arrival. Any difference in these times will introduce phase difference between the waves at each detector in the pair.

The horizon distance is how far the detectors are each able to see, depending on their sensitivity at each point in time, and thus alter the log likelihoods, while the set of detectors operable at the time of detection will alter the log likelihood as more detectors operable will be able to constrain sky localisation and coincidence criterion. The consistency check ξ_i^2 is important to distinguish between high SNR glitches that have a large residual between the glitch waveform and the template versus a well-matching signal.

For an injection run performed covering the full BBH and BNS parameter space, the probability density function (PDF) can be found for each $\Delta\phi$ and Δt. This is shown in figure 10 for the Hanford and Livingston detectors, discarding values where $|\Delta t| > 10$ms as this is the maximum time of travel at the speed of light between these two detectors.

Thus, the ranking statistic $\mathscr{L}$ is modified to boost rankings of high probability $\Delta\phi - \Delta t$ values, which would be the blue areas in figure 10. In lensing, the sky location constraint will alter the PDF of $\Delta\phi$ and present more red areas of the parameter space that are less likely to give true signals. Therefore this constraint can be built in to the current GstLAL TESLA pipeline to boost the ranking of signals which are closer in sky location and thus refine the search for lensed gravitational waves.

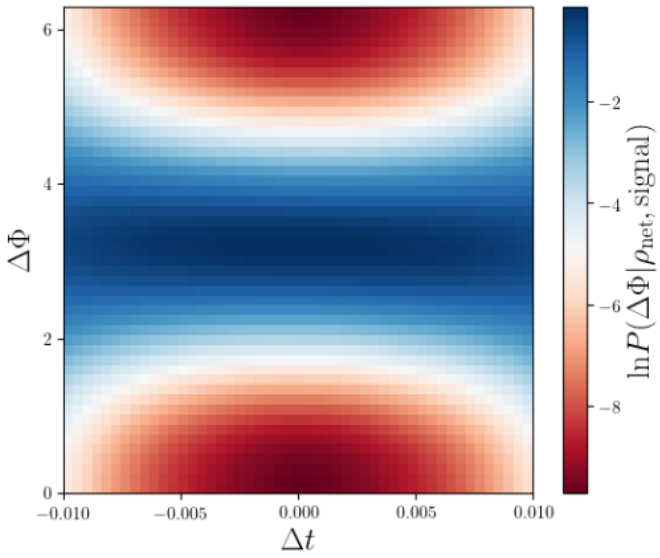

Figure 10. The probability distribution function $P(\Delta\phi|\Delta t,\rho_{network})$ across $\Delta\phi$ and Δt parameter space, $\rho_{network} = \sqrt{\rho_1^2+\rho_2^2}$ and $\rho_{H1} = \rho_{L1} = 10$. Figure from [21].

4. TIME PLAN

Date	Aims
May 15th	Finish and submit project proposal
May 15th to June 15th	-Extra preparation and reading, including learning more about Bayesian Analysis. -Understand how the GSTLaL pipeline works and perform a GSTLaL test run
June 15th to July 2nd (Week 1-3)	- Investigate how the waveform approximant affects the efficiancy of the targeted sub-threshold search,including understanding the difference between several approximants, test the match between approximants. - Work on interim report 1
July 2nd (Week 3)	Submit interim report 1
July 6th - August 20th	- Work on imposing a constraint on the skylocation of lensed images, including making changes to the GSTLaL pipeline. -Potentially start work on implementing a quasi-real-time lensing search which would use unclustered data to not have to match filter the data twice. - Work on Interim report 2, and then gather final results and make the final presentation
July 26- August 1, (Week 7)	Submit Interim Report 2 and Abstract
August 18-20 (Week 10)	Final Presentation
September 24	Final Report Due

5. PROGRESS UPDATE 1

It can be argued that the a bad fitting waveform family used to calculate the strain evolution of a gravitational wave could lead to lensed signals being missed in the pipeline. One of the main differences between these waveform families is whether they consider precession. Spin-aligned waveforms take the spin of the merging objects to be in the same direction as the orbital angular momentum, while precessing waveforms take any spin to calculate the strain of the gravitational waves. Two parameters are used to define the in-plane spin and spin-aligned components of the spin, named χ_P and χ_{eff} respectively and defined as:

$$\chi_P = max[\chi_1 sin\Theta_1, (\frac{4q+3}{4+3q})q\chi_2 sin\Theta_2] \ , \tag{20}$$

$$\chi_{eff} = \frac{\chi_1 cos\Theta_1 + q\chi_2 cos\Theta_2}{1+q} \ , \tag{21}$$

where χ_1 and χ_2 are the dimensionless component spins of both objects, Θ_1 and Θ_2 are the misalignment angles between the coponent spins and the orbital angular momentum, and q is the mass ratio of the merger.

All previously recorded super-threshold signals for O1, O2, and O3a have already recovered from previous lensing searches using both precessing and spin-aligned waveform families within the search pipelines. However, it is still necessary to investigate whether the sub-threshold signals would be effectively recovered with the same SNR using either waveform.

To do this, I found the match between precessing and spin-aligned waveforms of previous gravitational wave events from O1 and O2. The BNS event GW170817 was disregarded as the lensing searches will primarily target BBH merger events, as they will be louder farther away and thus are more likely to have lensing masses along the line of sight from the event to Earth.

Firstly, the maximum posterior was found for each of the 15 parameters of the merger, where the posterior samples were found from [27], and the maximum likelihood posterior sample found to calculate the match, as these samples are the ones that best fit the data. Two sets of these posteriors were found for each event, one for spin-aligned posteriors and one for effective precession posteriors.

The antenna pattern function was also considered in order to calculate the actual strain response in the detector. The detector response for each polarisation and each detector d, $F_{+,d}$ and $F_{\times,d}$, were combined with the strain for each polarisation, h_+ and $h_\times$ to give the total antenna response for each detector h_{tot}:

$$h_{tot,d} = F_{+,d} \times h_+ + F_{\times,d} \times h_\times . \tag{22}$$

The waveforms were then generated in each detector for each h_{tot} using both a spin-aligned waveform family, `SEOBNRv2` and an effective precession family, `IMRPhenomPv2`, as shown for GW170104 in figure 11. The matches between these two waveforms found with `pycbc` and the average results between detectors from these matches found and plotted in figure 12.

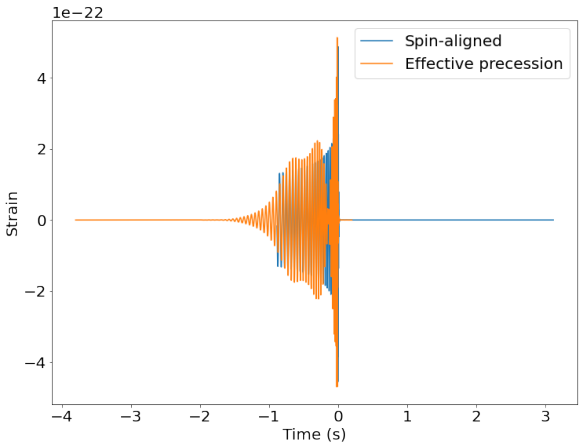

Figure 11. The time domain waveforms for GW170104 as seen in the Hanford detector, calculated using spin-aligned waveform family SEOBNRv2 in blue and precession-included waveform family IMRPhenomPv2 in orange. The precessing waveform displays obvious signs of amplitude modulation. The match between these two waveforms was 58%.

It was found that while many of the events were above 90% match between waveforms, GW170104 exhibited a lower average match of 54%. It is possible that this merger was therefore precessing. It could be that posterior distribution for the in-plane spin components of each body χ_P may be wide around the maximum posterior, and therefore it cannot be determined if the orbit is precessing. If this were the case then there may not necessarily be SNR loss between the two waveform families. However, if the system was definitely precessing, with a narrow χ_P distribution around some non-zero value, the precessing waveform would be truer match to the signal, and thus the choice of a spin-align waveform family could incur a 46% loss in SNR for the match of 54%. Thus it would be important to choose a precessing waveform in this case. However, with current methods the spin parameter is not often measured this precisely. To investigate this further, I would look at the posterior distributions of the parameter χ_P for the lower match event and look into how reliably it can be said that a merger is precessing in order to further qualify the necessity of a precessing waveform with the current measurements of spin.

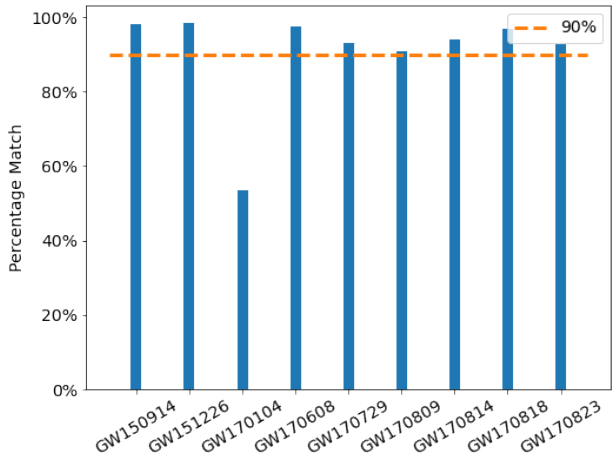

Figure 12. The average match from both Hanford and Livingston detectors between spin-aligned and precessing waveform families. Eight of the events have a $> 90\%$ match, although GW170104 displays a match of approximately 53%. This event could be precessing and therefore not well defined by a spin-aligned waveform. This could cause problems in the sub-threshold lensing search if a spin-aligned waveform is used to search for a precessing sub-threshold signal, as it may incur heavy SNR loss.

PROGRESS UPDATE 2

For a given set of detectors, sensitivity, and signal, the probability of obtaining the SNR, phase and time difference between detectors obeys the following probability:

$$P(\vec{\rho},\vec{\phi},\vec{t}|\vec{d},\vec{D},signal) \propto P(ln\vec{D}_{eff},\vec{\Delta\phi},\vec{\Delta t}|\vec{d},signal) \times |\vec{\rho}|^{-4}. \tag{23}$$

Where each vector is said quantity at each detector, or for $\vec{\Delta\phi}$ and $\vec{\Delta t}$ between each detector, quantities corresponding to the values as stated for equation 19. D_{eff} is the effective distance to the signal source and can be used to estimate the probability due to the relationship:

$$\rho = \frac{1}{D_{eff}}. \tag{24}$$

The factor of $|\rho|^{-4}$, where $|\rho|$ is the detector network SNR, comes from the probability of observing a signal at a distance D over an area dD is proportional to $D^2 dD$. The probability of observing a signal of some SNR ρ is then proportional to ρ^{-4}.

In GstLAL, the probability given on the right-hand side of equaition 23 is evaluated with a further simplification involving the gridding of points across the sky as well as the covariance matrix which contains information on the variances between time, phase and effective distance [28]. I have so far altered the gridding section of the GstLAL code to take a skymap of a previous event and grid evenly over only the region of the sky given by the 90% credible region of this event. The probability of each $\vec{\Delta\phi}$ and $\vec{\Delta t}$ will then be evaluated as before and plotted as in figure 10 for each detector pair. This then needs to be implemented into the TESLA pipeline.

[a] storm.colloms@ligo.org
[b] kli7@caltech.edu
[c] ajw@caltech.edu

[1] B. Abbott, R. Abbott, T. Abbott, M. Abernathy, F. Acernese, K. Ackley, C. Adams, T. Adams, P. Addesso, R. Adhikari, and et al., Physical Review Letters **116** (2016), 10.1103/physrevlett.116.241102.
[2] B. Abbott, R. Abbott, T. Abbott, S. Abraham, F. Acernese, K. Ackley, C. Adams, R. Adhikari, V. Adya, C. Affeldt, and et al., Physical Review X **9** (2019), 10.1103/physrevx.9.031040.
[3] R. Abbott, T. D. Abbott, S. Abraham, F. Acernese, K. Ackley, A. Adams, C. Adams, R. X. Adhikari, V. B. Adya, and et al., "Gwtc-2: Compact binary coalescences observed by ligo and virgo during the first half of the third observing run," (2021), arXiv:2010.14527 [gr-qc].
[4] D. Kennefick, Physics Today - PHYS TODAY **62** (2009), 10.1063/1.3099578.
[5] O. A. Hannuksela, K. Haris, K. K. Y. Ng, S. Kumar, A. K. Mehta, D. Keitel, T. G. F. Li, and P. Ajith, The Astrophysical Journal **874**, L2 (2019).
[6] C. McIsaac, D. Keitel, T. Collett, I. Harry, S. Mozzon, O. Edy, and D. Bacon, Physical Review D **102** (2020), 10.1103/physrevd.102.084031.
[7] A. K. Y. Li, R. K. L. Lo, S. Sachdev, C. L. Chan, E. T. Lin, T. G. F. Li, and A. J. Weinstein, "Finding diamonds in the rough: Targeted sub-threshold search for strongly-lensed gravitational-wave events," (2021), arXiv:1904.06020 [gr-qc].
[8] K. Haris, A. K. Mehta, S. Kumar, T. Venumadhav, and P. Ajith, "Identifying strongly lensed gravitational wave signals from binary black hole mergers," (2018), arXiv:1807.07062 [gr-qc].
[9] J. M. Ezquiaga, D. E. Holz, W. Hu, M. Lagos, and R. M. Wald, Physical Review D **103** (2021), 10.1103/physrevd.103.064047.
[10] J. M. Ezquiaga and M. Zumalacárregui, Physical Review D **102** (2020), 10.1103/physrevd.102.124048.
[11] K. Kim, J. Lee, R. S. H. Yuen, O. A. Hannuksela, and T. G. F. Li, "Identification of lensed gravitational waves with deep learning," (2020), arXiv:2010.12093 [gr-qc].
[12] K.-H. Lai, O. A. Hannuksela, A. Herrera-Martín, J. M. Diego, T. Broadhurst, and T. G. Li, Physical Review D **98** (2018), 10.1103/physrevd.98.083005.
[13] R. Takahashi and T. Nakamura, The Astrophysical Journal **595**, 1039–1051 (2003).
[14] A. Einstein and M. Grossmann, Zeitschrift für Mathematik und Physik (1914).
[15] F.-G.-R.-B.-M. LIGO-Scientific-Collaboration, Virgo-Collaboration and INTEGRAL, The Astrophysical Journal Letters **848** (2017), 10.3847/2041-8213/aa920c.
[16] T. G. F. Li, *Extracting Physics from Gravitational Waves: Testing the Strong-field Dynamics of General Relativity and Inferring the Large-scale Structure of the Universe*, Ph.D. thesis, Vrije U., Amsterdam (2013).
[17] B. P. Abbott, R. Abbott, T. D. Abbott, M. R. Abernathy, and F. Acernese (LIGO Scientific Collaboration and Virgo Collaboration), Phys. Rev. Lett. **116**, 061102 (2016).
[18] B. Abbott, R. Abbott, T. Abbott, M. Abernathy, F. Acernese, K. Ackley, C. Adams, T. Adams, P. Addesso, R. Adhikari,

and et al., Physical Review Letters **116** (2016), 10.1103/physrevlett.116.061102.

[19] L. Caltech, "Sources and types of gravitational waves," .

[20] B. Abbott, R. Abbott, T. Abbott, M. Abernathy, F. Acernese, K. Ackley, C. Adams, T. Adams, P. Addesso, R. Adhikari, and et al., Physical Review Letters **116** (2016), 10.1103/physrevlett.116.241103.

[21] S. Sachdev, S. Caudill, H. Fong, R. K. L. Lo, C. Messick, D. Mukherjee, R. Magee, L. Tsukada, K. Blackburn, P. Brady, P. Brockill, K. Cannon, S. J. Chamberlin, D. Chatterjee, J. D. E. Creighton, P. Godwin, A. Gupta, C. Hanna, S. Kapadia, R. N. Lang, T. G. F. Li, D. Meacher, A. Pace, S. Privitera, L. Sadeghian, L. Wade, M. Wade, A. Weinstein, and S. L. Xiao, "The gstlal search analysis methods for compact binary mergers in advanced ligo's second and advanced virgo's first observing runs," (2019), arXiv:1901.08580 [gr-qc].

[22] C. Messick, K. Blackburn, P. Brady, P. Brockill, K. Cannon, R. Cariou, S. Caudill, S. J. Chamberlin, J. D. Creighton, R. Everett, and et al., Physical Review D **95** (2017), 10.1103/physrevd.95.042001.

[23] R. Narayan and M. Bartelmann, "Lectures on gravitational lensing," (2008).

[24] M. Oguri, Monthly Notices of the Royal Astronomical Society **480**, 3842–3855 (2018).

[25] S.-S. Li, S. Mao, Y. Zhao, and Y. Lu, Monthly Notices of the Royal Astronomical Society **476**, 2220–2229 (2018).

[26] K. K. Ng, K. W. Wong, T. Broadhurst, and T. G. Li, Physical Review D **97** (2018), 10.1103/physrevd.97.023012.

[27] "Pe event samples," (2021).

[28] C. Hanna, S. Caudill, C. Messick, A. Reza, S. Sachdev, L. Tsukada, K. Cannon, K. Blackburn, J. D. Creighton, H. Fong, and et al., Physical Review D **101** (2020), 10.1103/physrevd.101.022003.